Forschungszentrum Karlsruhe
in der Helmholtz-Gemeinschaft

Wissenschaftliche Berichte
FZKA 7329

Semi-Mechanistic Approach for the Kinetic Evaluation of Experiments on the Oxidation of Zirconium Alloys

G. Schanz

Institut für Materialforschung
Programm Nukleare Sicherheitsforschung

August 2007

Forschungszentrum Karlsruhe

in der Helmholtz-Gemeinschaft

Wissenschaftliche Berichte

FZKA 7329

Semi-Mechanistic Approach for the Kinetic Evaluation of Experiments on the Oxidation of Zirconium Alloys

G. Schanz

Institut für Materialforschung
Programm Nukleare Sicherheitsforschung

Forschungszentrum Karlsruhe GmbH, Karlsruhe

2007

Forschungszentrum Karlsruhe GmbH
Postfach 3640, 76021 Karlsruhe

Mitglied der Hermann von Helmholtz-Gemeinschaft
Deutscher Forschungszentren (HGF)

ISSN 0947-8620

urn:nbn:de:0005-073297

Verfahren mit mechanistischem Ansatz für die kinetische Auswertung von Experimenten zur Oxidation von Zirkonium-Legierungen

Kurzfassung

Die Kinetik der Oxidation von Zirkonium und Zr-Legierungen kann durch das Phänomen des so genannten breakaway in Abhängigkeit von verschiedenen Einsatzbedingungen und dem Medium wesentlich beeinflusst werden. Obwohl Ergebnisse mechanistischer Untersuchungen aus mehreren Jahrzehnten vorliegen, ist bis heute noch kein Einverständnis über die Bedeutung verschiedener sich gegenseitig beeinflussender Parameter erreicht. Jedoch scheinen kürzlich durchgeführte vertiefte Untersuchungen bestätigt zu haben, dass die Wachstumskinetik von Oxidschichten insgesamt von den Alterungsbedingungen des Verbands von Oxid-Teilschichten abhängt, denen diese seit ihrer Bildung unterliegen. Es ist bekannt, dass unter speziellen Bedingungen auch örtliche Variationen im Wachstum und dem mechanischen Versagen von Oxidschichten auftreten können. Dieses komplexe Verhalten ist für die kerntechnische Industrie von großer technischer und wirtschaftlicher Bedeutung.

Eine Auswertung experimenteller Ergebnisse auf halb-mechanistischer Grundlage wird vorgestellt. Dieser neue Ansatz verbindet die Anpassung an experimentelle Daten mit einer analytischen Behandlung, die es erlaubt einen bestimmten mechanistischen Befund in vereinfachter Form zu beschreiben: Dem Fortschreiten der im Temperaturbereich der beobachteten breakaway Anomalien nachgewiesenen Umwandlung von Oxid mit tetragonaler Kristallstruktur in die monokline Modifikation wird durch die Annahme kubischer Kinetik Rechnung getragen. Mit dieser Simulation wird im Vorfeld des bisher berücksichtigten Post-transition- Gebiets ein Pre-transition-Gebiet definiert. Der Formalismus folgt dem vereinfachten Konzept der Verwendung von Korrelationen, um temperatur-transiente Rechnungen zu erleichtern. Anstatt weitere und willkürliche Koeffizienten für Oxidationsgeschwindigkeiten einzuführen, werden die durch den breakaway verursachten Anomalien mit den resultierenden Bereichsgrenzen verknüpft, so dass die grundsätzliche Kinetik und die kinetischen Folgen des breakaway separat diskutiert werden können.

Die Auswertungsmethode wird als Referenz für Zry-4/Dampf angeboten, ohne den Anspruch zu erheben, mit den bereitgestellten Bereichsgrenzen für den breakaway die optimale Anpassung an die gesamte experimentelle Datenbasis gefunden zu haben. Die angeregte Anpassung des Verfahrens auf andere Legierungen und Medien erfordert hinreichend umfangreiche Datensätze, um zuverlässige Auswertungen zu ermöglichen und Quervergleiche anstellen zu können.

Abstract

The oxidation kinetics of zirconium and Zr-alloys can be influenced essentially by the so-called breakaway phenomenon, depending on various exposure conditions and the medium. Mechanistic investigation results gained during decades up to now have not yet provided an agreement on the importance of several interfering parameters. However, recently performed sophisticated studies seem to have confirmed, that the growth kinetics of oxide scales in total depends on the aging conditions provided for the compound of scale sub-layers since their individual formation. Local variations of scale growth and mechanical failure are also known to occur under special conditions. This complex behavior is highly relevant for the nuclear industry in technical and commercial respect.

A semi-mechanistic evaluation of experimental results is presented. This novel approach combines fitting to experimental data with an analytical treatment, allowing to describe a certain mechanistic fact in simplified form: The ongoing transformation of tetragonal oxide into the monoclinic modification during scale growth within the temperature range of observed breakaway anomalies is simulated by assumed cubic mass gain kinetics. Thus a pre-transition regime is defined in advance of the post-transition regime, taken into account up to now. The formalism follows the simplification of a correlations concept, in order to facilitate temperature transient calculations. Instead of introducing additional and arbitrary oxidation rate coefficients, the breakaway anomalies are formally linked to the resulting regime boundaries, so that basic kinetics and breakaway response can be discussed separately.

The evaluation procedure is offered as reference for Zry-4/steam, without claiming, that the optimum fit to all available experimental data has been found with the provided breakaway regime boundary data. The encouraged adaptation of the procedure to other alloys and exposure media requires sufficiently large data sets for reliable evaluations and cross comparison purposes.

TABLE OF CONTENTS

1 Introduction 1

2 Review of Experimental Results 1
2.1 Oxidation kinetics for steam and water 1
2.2 Breakaway phenomena 3
2.3 Mechanistic results and tentative interpretation 5

3 Analytical Treatment 7
3.1 Approach 7
3.2 Calculation method 9
3.3 Data input and fitting 9
3.4 Results 11
3.5 Discussion 19

4 References 20

Annex A: Examples of the developed SigmaPlot®, ©SPSS Inc. user-defined transforms 22

LIST OF FIGURES

Fig. 1: Boundaries of the kinetic regimes within the temperature vs. mass gain field, determined in the fitting procedure

Fig. 2: Comparison of mass gain vs. time between a partial set of experiments (data points unpublished results included in [Leis1983]) and calculations (curves) for the temperature range 1373 to 1173 K

Fig. 3: Comparison of mass gain vs. time between a set of experiments (data points [Leis1983]) and calculations (curves) for the temperature range 1123 to 873 K

Fig. 4: Comparison of the correlations according to Dyce-Stehle and Van der Linde for the description of autoclave test results (dashed correlations and transition boundary lines as cited in [Garz1980]) with calculated results (full lines)

Fig. 5: Comparison of the correlations according to Hillner and Dalgaard for the description of autoclave test results (dashed correlations and transition boundary line as cited in [Garz1980]) with calculated results (full lines)

Fig. 6: Verification of the consistent calculation of mass gain progress during the temperature-transient phases of three idealized exposure temperature histories, remaining below or passing beyond breakaway regime temperature limits, respectively

1 Introduction

Excellent performance properties of presently available LWR fuel rod claddings reflect the achievements of zirconium alloy development and the acquired knowledge on adequate service conditions. The huge base of published results, proprietary data, and experience can be exploited for a refined interpretation of the complex oxidation phenomena, which is needed for future, more challenging application conditions. The paper is to offer a novel semi-mechanistic approach for the evaluation of experimental results on the oxidation kinetics of zirconium alloys in oxidizing media. The developed procedure is focused on anomalies related to the breakaway phenomenon, realized prior to the kinetic transition during the oxidation of Zircaloy-4 in steam, and helps to distinguish those effects from the regime of “normal” oxidation progress. The aims of this approach are to separate basic and general parameters from breakaway related ones, to identify reasons for eventual discrepancies between mechanistic assumptions and experimental facts, as well as to encourage further mechanistic studies. Tentative application to other zirconium alloys and different media is recommended. The general message, however, shall be to support the common features of Zr oxidation kinetics independent of temperature range and medium.

Basically, the oxidation of Zr alloys in various oxidizing media is quite similar, despite the fact that specific features may depend strongly on material composition and state, medium, temperature range, irradiation, and other conditions of exposure. Mechanistic information is insufficient e.g. in two fields: 1) The phenomena involved in the breakaway transition and the associated enhancement of hydrogen pick-up are still controversially discussed for advanced LWR claddings and water chemistry specifications. 2) The evaluation of the risks of air ingress in spent fuel storage and severe fuel damage (SFD) scenarios requires kinetic and mechanistic information on sequential and mixed steam/air exposure. The complex interference of breakaway similar features and nitrogen specific effects of air exposure is not considered here, but the comparison of air and steam might facilitate the separation of the influencing factors and thus the task to formulate a mechanistic model.

2 Review of Experimental Results

2.1 Oxidation kinetics for steam and water

The most adequate analytical description of Zr alloys oxidation kinetics is based on the solution of the oxygen diffusion problem for the finite solid state system and the adjacent medium, and the use of phase diagram and diffusion data as input [Vesh1997]. The kinetics of the oxygen uptake (mass gain), the growth of ZrO_2 scale and α-Zr(O) layer, and the oxygen transfer to the matrix are thus provided. One kind of anomalies of oxygen concentration profile and layers growth kinetics, observed in fast temperature transients, was interpreted by the interim formation of a two-phase layer beneath the oxide as result of non-equilibrium boundary concentration profiles [Sawa1977], and this can be taken into account in a mechanistic code.

Other anomalies in scale growth kinetics and their unexpected system pressure dependence were explained by a hysteresis of the martensitic transformation between the tetragonal and the monoclinic modification of zirconia (ZrO_2 t/m transformation) [Paw1977]). This transformation will play a major role in the present paper in other respect.

For the high temperature range, SFD codes of integral type rely generally on a simplified treatment of the steam oxidation, neglecting limited system geometry and anomalies: In those the oxidation is described using reaction rate functions of parabolic time and Arrhenius temperature dependence. Recently a set of correlations was recommended, based on the critical review of experimental data [Scha2003], their statistical evaluation within the diffusion system concept, and their verification against rod bundle experiments [Vol2004].

Long-term Zry-4/steam oxidation was systematically studied in the temperature range 1373 to 873 K with respect to deviations from parabolic towards cubic rates, the breakaway transition, and the post-transition kinetics [Leis1983, Leis1985, and unpublished details]. “Normal” oxidation behavior was found for 1373 K, confirmed for massively oxidized rods instead of tube specimens. In contrast, similar tests at 1323 K identified a rather late breakaway transition, and related changes in the scale microstructure. Accordingly, the “transition regime boundary temperature” can be set to ~1350 K. Deviations from parabolic rates arise below ~1300 K and gain importance with decreasing temperature. A comparison of mass gain with scale and α-Zr(O) layer growth reveals anomalous trends in the relations between those data. At 1273 K the ZrO_2 to α-Zr(O) thickness ratio decreases with time until the onset of the breakaway transition. The distinction of α-Zr(O) layer and α-Zr matrix, which is also possible below ~1093 K, indicates a similar trend for the lower temperatures. Features of a subsequent transition were found in the whole covered temperature range, including some scoping tests down to 673 K. A decrease of the “critical” scale thickness with decreasing temperature was continuous in the whole studied range, whereas a minimum of the “critical” time to transition was found at 1273 K. Apart from the temperature range of the (α+β)-Zr phase coexistence (1093 to 1243 K for native Zry-4), the ZrO_2 to α-Zr(O) thickness ratio increases abruptly within the post-transition regime. Parallel to the fast growth of defective scale, a quasi stationary equilibrium between α-Zr(O) inward growth and external consumption results in stationary but somewhat temperature dependent α-Zr(O) thickness values. Within the two-phase range, for experiments at 1123, 1173, and 1223 K, a gentle transition of mass gain was accompanied by localized scale growth transition leading to the formation of oxide pustules.

Under exposure to pressurized water in autoclave experiments, zirconium alloys oxidation shows the transition from essentially cubic to linear kinetics at temperature dependent critical scale thicknesses of typically a few microns. The evaluation of different sets of experimental data resulted in the formulation of (simply empirical) ex-reactor corrosion models as those according to Hillner (~530 to 670 K, cubic pre-transition and linear post-transition kinetics), the two corresponding correlation sets of Van der Linde and Dyce, and the Dalgaard “long-term” model (573 to 673 K, pre-transition neglected, linear kinetics). Those activities and correlations are reviewed in [Garz1980] and have been used in that paper for comparison purposes:

[Garz1980] established a data base of Zircaloy corrosion results under PWR operating conditions. The given evaluation of the data was compared to the above mentioned empirical ex-reactor corrosion models. The generally registered surplus of in-reactor corrosion over ex-reactor rates was expressed in form of fitting factors. Those factors were found to depend on characteristics of certain plants and even cycles, and were discussed in relation to the thermal conductivity of the growing scale and the indirect kinetic influence under heat flux conditions.

A review by B. Cox [Cox2005] on Zr in-reactor corrosion is concentrated on those studies that have resulted in changed views of the importance of various mechanisms. The author concludes that the hypothesis of in-reactor corrosion rate enhancement as direct result of displacement damage by fast neutron bombardment is not sufficiently supported. Indirect influences seem to be better established, e.g. the enhanced Fe redistribution from second phase particles (SPPs) under fast neutron recoil damage. Advanced alloys with improved corrosion resistance in PWRs are generally low in Fe (and Sn) or have Fe in form of more radiation resistant SPPs than those in the Zircaloys. A direct effect of radiation as cause of nodular corrosion in BWRs is also not supported by the author. Instead, the suppression of irradiation induced redistribution of Fe from SPPs into the Zr matrix is seen to have contributed to the successful elimination of nodular corrosion susceptibility of Zircaloys. Galvanic reasons for both, nodular corrosion and shadow corrosion are reported to be evident.

Cox [Cox2005] gives the following comment: “If the oxidation mechanism out-reactor is not understood, useful interpretations of the in-reactor behavior cannot be offered”. In the focus of interest at present are advanced alloys, water chemistry specification and control, and the potentials for extensions of service temperature, rod power, and discharge burn up (see e.g. various contributions to [ANS2004]).

2.2 Breakaway phenomena

The term “breakaway effect” is used here for mechanistic aspects of phenomena, which may proceed coupled at the whole sample surface. But also included shall be similar localized effects as e.g. the “nodular corrosion” (earlier BWR and SGHWR experience), and a moderate form of lateral spreading of oxide pustules, resulting in a gentle kinetic transition (steam exposure within the (α+β)-Zr two-phase range, as mentioned in the previous chapter [Leis1983, Leis1985]). The terms “pre-transition” and “post-transition” are preferred for denomination of the resulting kinetics for the respective regimes. For clarity some introductory comments are added: A coarse classification of the aspects, observed in relation to the breakaway effect, can distinguish changes in scale and metal microstructure, features of mechanical scale cracking and delamination, and kinetic responses. Apart from the coupling to the metallic substrate, many scale conditions and properties as compressive stress, shear stress, stress relaxation, lattice substoichiometry and impurities, and growth defects may interfere. For this reason the most direct investigation methods as e.g. X-ray diffraction measurements at temperature and during scale growth are to be preferred. Results gained for ceramic specimens cannot be applied directly to the investigation of growing scales.

Several reviews providing breakaway related results and discussions are available. In a review article [Ahm1975], the dispute between promoters of microstructure-related and fracture-related causalities is stressed. The mechanistic investigations by B. Cox on zirconium alloy corrosion, for which a spectrum of experimental and analytical methods has been applied, shall be especially mentioned [Cox1976]. In the above cited recent review [Cox2005], three forms of observed transition are distinguished: (1) Quite sudden transition followed by post-transitional cycles or steady post-transition rate increase. (2) More gentle change from cubic to enhanced linear kinetics. (3) Slow transition, either fast nucleating but slowly spreading, or as genuinely slow and uniform process. The third variant is described as “para-linear”, involving the sequence of cubic, parabolic, and linear sections.

The presented paper is focused on some aspects of the breakaway effect, which are addressed in more detail. A publication by T. Nakayama and T. Koizumi [Naka1967] reports about oxidation experiments, carried out in oxygen and air in the temperature range 673 to 1423 K, for reactor grade Zr, commercial grade Zr-2.4Hf, Zry-2, Zr-Sn (1.5 and 3.0), and Zr-Ti (1.5 and 3.0). The oxidation kinetics was recorded in thermo-balance tests. Metallographic specimen cross section inspection and oxide phase analysis by X-ray diffraction were performed before and after the breakaway transition. Moreover, the structure of growing scale was recorded in high-temperature X-ray diffraction studies at various temperatures during oxidation, in order to identify the “aging” of the scale close to its surface. For comparison, the phase transformation hysteresis of oxide powder was studied by differential thermal analysis.

Following the idea, that the polymorphic transformation of tetragonal (metastable below 1423 K) to monoclinic ZrO_2 might play a major role in the breakaway phenomenon, the authors seem to be pioneers to have detected the continuous transformation of initially duplex phase oxide (with considerable fraction of metastable tetragonal phase near to the metal interface) towards the monoclinic phase (near to the surface) in the further growth of the scale and during the loss of its dark color. The promoted transition in the Sn- and Ti-containing alloys compared to reactor grade Zr is seen in relation to a stabilization of the tetragonal phase to the lower temperatures due to those alloying elements. No direct correlation of the continuous phase transformation trend with the quite abrupt transition is found. The tendency of retarded scale growth before the transition, seen in several of the presented kinetic curves, is a remarkable observation. The comparison of several materials under oxygen exposure is valuable, whereas only some results on the complex behavior in air (interference of nitrogen) are given.

2.3 Mechanistic results and tentative interpretation

The following discussion deals with the ongoing phase transformation within the ZrO_2 scale from the originally tetragonal to the monoclinic modification (ZrO_2 t/m phase transformation) in relation to the relaxation of compressive scale growth stress and the oxide grain coarsening during oxidation. Consequently, phase composition profiles across the scale, residual stress, and grain size are regarded. Progress and hysteresis of the t/m transformation of martensitic type may depend on many parameters, for which a direct study is difficult.

The above cited own experimental data [Leis1983, Leis1985, and unpublished details] were favorable for metallographic specimen evaluation due to the coarse features of the scale degradation observed at high temperatures. A tentative interpretation of the results was given [Sch1981, Scha1981], in which arguments discussed at that time were adapted, and conflicting theories could be reconciled. Accordingly, the breakaway effect should be caused by the ZrO_2 t/m phase transformation, whereas the scale degradation and the kinetic transition should follow as consequences. The retention of t-ZrO_2 below the stability temperature range was seen to be due to high compressive stress, small grain size, and the substoichiometry of fresh oxide. Accordingly, phenomena observed in advance of the kinetic transition have to be included in the interpretation of the breakaway effect. It is just claimed that the given mechanistic interpretation is self-consistent and reasonable for the set of experiments from which they were derived. For various other conditions, for which the relevance of this mechanistic breakaway model is open, modifications or the inclusion of further parameters may be required. This need is especially seen for cases of competition between two reactive species as oxygen plus hydrogen in steam or water, and oxygen plus nitrogen in air. The localized onset of scale degradation and the moderate forms of transition and post-transition kinetics for Zry-4/steam at 1123, 1173, and 1223 K (within the range of the (α+β)-Zr phase mixture), were already mentioned [Leis1983, Leis1985]. Duplex phase Zry-4 is known to show superplastic matrix strain, allowing relief of scale growth stress during tube oxidation. This may be the reason for the observed smaller pick-up fraction of hydrogen (a β-Zr stabilizer) within the temperature range of duplex phase matrix.

The well known tendency in the time dependence of the oxidation kinetics of zirconium alloys at medium to lower temperatures to deviate from parabolic towards cubic scale growth is discussed by Sabol et al. [Sabo1975] to result from the decreasing relative contribution of grain boundary diffusion during grain coarsening with time. Following this argument, an extra boundary diffusion related contribution during the initial oxidation would be expected.

Meanwhile quite a lot of information has become available. A part of the publications seem to support the main importance of the t/m transformation of ZrO_2. Roy et al. [Roy1970] report about the coexistence of the tetragonal and the monoclinic phase in oxide films grown in high temperature high pressure water. Godlewski et al. [Godl1991], [Godl1994] confirm this observation. Accordingly, t-ZrO_2, stable above 1423 K, is stabilized to lower temperatures by compressive stress. The authors identify the higher t-fraction in t+m oxide at the oxide/metal interface compared to the scale surface. They argue about a positive influence on the corrosion resistance of Zr alloys, and describe t-ZrO_2 as the minor constituent, irregularly distributed within m-ZrO_2. Niobium is reported to decrease the stability of t-ZrO_2 in Zr-1.0Nb alloys [Kim1990], whereas Fe and Sn are stated to stabilize t-ZrO_2 near $Zr(Fe,Cr)_2$ precipitates

[Li1994]. Godlewski et al. [Godl2000] perform a Raman spectroscopy study towards the stress gradient across oxide scale, and obtain a distribution of compressive stress (1.5 GPa to 800 MPa) in reasonable correlation with the profile of t-ZrO_2.

According to a literature survey, Barberis [Barb1995] classifies the hypotheses proposed to explain the low temperature stabilization of the tetragonal phase into three groups:

- Grain sizes below 20-30 nm
- Point defects (related to oxygen substoichiometry and dopants)
- Compressive stresses

In his own X-ray investigation, Barberis reports on the evolution of the allotropic phase transformation of oxide films on zirconium alloys during autoclave tests at 400 and 500 °C. In this study, a Zry-4 type alloy with 1.2 % Sn is compared to a corresponding tin-free alloy, the phase composition is calculated from the diffraction peak intensities, and the grain sizes from the peak widths. The well known and industrially important influence of the tin content is confirmed by the increased corrosion resistance and the retarded transition of the tin-free alloy. The fraction of tetragonal phase is found to decrease with increasing duration of exposure from original values of roughly 10 %, and the grain size of the monoclinic constituent is reported to increase similarly for both alloys.

Commercial high-purity nanocrystalline zirconia powder, autoclave exposed in parallel, served as reference for the oxide films, since not influenced by stresses and changing substoichiometry. With the duration of powder exposure, the zirconia showed a steady decrease of the tetragonal phase fraction starting from ca. 85 % and a fast grain growth of both phase constituents from ca. 15 nm to ca. 25 nm. According to the obtained relation between tetragonal phase content and grain size, a critical value of ca. 30 nm was deduced, above which the tetragonal phase should be unstable. The fraction of tetragonal phase in zirconia powder as function of exposure duration and temperature was fitted to the Johnson Mehl Avrami (JMA) correlation and the resulting parameters were applied to the oxide film results: In the evaluation for the scales, constant tetragonal phase fraction at time of formation of the differential sub-layer and independence from the alloy composition is assumed. Predicted is a steeply beginning and monotonously leveling gradient of tetragonal phase amount from the metal/oxide interface (high) to the surface (low) and an increase of the corrosion resistance with decreasing tetragonal phase fraction for a given scale thickness. The absolute value of the tetragonal phase fraction at the metal/scale interface is estimated to be 35 % for both alloys. The transition-related oxidation rate acceleration is accompanied by a slower further decrease of the tetragonal fraction but not by an abrupt change. The comparative discussion with literature results includes possible influences of hydrogen (protons in the scale). Barberis [Barb1995] concludes that the grain size is the factor which mainly determines the fraction and distribution of the tetragonal zirconia phase during the studied zirconium alloys oxidation, whereas the role of stresses and dopants cannot be ruled out.

Park et al. [Park2004] have exposed recrystallized Zr-1.5Nb and stress-relieved Zry-4 to pure water at 360 °C and 18.5 MPa (according to ASTM G2-88) for up to 300 days. Oxide layers of ~4 µm (~60 mg/dm^2), formed within 150 days were examined by TEM-EDX in cross section and analyzed for phase composition and grain size in a micro-beam X-ray investigation using a synchrotron radiation source. Mixtures of monoclinic and tetragonal phase with grain sizes of about 25 to 30 nm are deduced for both alloys, with the smaller size for the tetragonal phase. Across the scales, gradients of the tetragonal phase fraction from ca. 15% at the metal interface to ca. 5% at the surface are calculated. For Zry-4, the tetragonal phase fraction is found to be retained to a larger distance from the interface (less steep gradient compared to Zr-1.5Nb). This is seen in relation to the earlier breakaway transition and the inferior corrosion resistance of this alloy on the long term. But the authors conclude, that the stabilization of the tetragonal fraction is not the decisive parameter for orientation on corrosion resistance.

For a transmission electron microscopy investigation by Yilmazbayhan et al. [Yilm2006], scales of Zry-4, ZIRLO, and Zr-2.5Nb were prepared as cross section foils. The scales were formed in standardized (ASTM G2-88) autoclave tests at 360 °C in pure and lithiated water. Depending on alloy, test duration, and medium, scales exhibit more or less periodic alternations between columnar grain morphology and zones with equiaxed grains and associated lateral cracks. The columnar grains are discussed as the more protective oxide growth variant, and cracking is interpreted as artifact. Referring to a previous synchrotron radiation study and based on X-ray diffraction peak broadening results, the authors see overall consistence for the idea, to correlate monoclinic or tetragonal structure with predominately columnar or small and equiaxed grain morphology, respectively. Detailed diffraction and texture evaluations indicate the preponderance of the monoclinic phase for the alloys in total, and the comparatively highest tetragonal fraction for Zry-4. Indications seem to confirm that the tetragonal modification of zirconia is stabilized by small crystallite size.

3 Analytical Treatment

3.1 Approach

The novel analytical procedure of treating anomalous kinetics has been presented at the 2006 ANS Annual Meeting (see summary [Scha2006]).

Normal oxidation: In general, the oxidation of zirconium alloys is determined by the oxygen uptake from the medium and its diffusive transport within the α-Zr or β-Zr alloy matrix and across the growing layers α-Zr(O) and ZrO_2. Following the often applied simplification, the rate of mass gain is described by a correlation with parabolic time and exponential (Arrhenius) temperature dependence, respectively. It is assumed that this treatment is adequate for the whole range of “normal” oxidation, in which the tetragonal ZrO_2 modification is formed. Tentatively this range includes the metastable extension of the tetragonal oxide phase field to low temperatures within the time limits, beyond which the breakaway related anomalies begin to arise. Those are assumed to be initiated by the onset of the t/m transformation of

ZrO_2. The approach is not applicable to starvation conditions, and the description of advanced tube wall conversion should be examined critically. One has to keep in mind that a correlations approach refers to unlimited supply of oxidant from the gas phase and to unlimited geometry of the solid system.

Pre-transition oxidation: As reported in the previous chapter, recent literature results confirm the ongoing transformation process from metastable tetragonal (t) to monoclinic (m) ZrO_2 during the pre-transition period. Such a trend should be accompanied by a decrease in oxygen diffusivity, according to the narrower substoichiometry range of m-ZrO_2. (Unfortunately, diffusion data for m-ZrO_2 are not available.) This trend is assumed here to be responsible for cubic time dependence of mass gain rate, following a reasonable procedure of treating other systems in certain transitional states. The pre-transition kinetics is to be closely linked to the normal kinetics, and the regime shall be determined by fitting to experimental data.

Post-transition oxidation: Common features of most experimental observations are the coupled lateral cracking and detachment of scale with “critical” thickness, and the quasi periodic repetition of such mechanical scale degradation. The protective properties of each new partial layer become lost, accordingly, on the average a linear time dependence of the post-transition rate should be valid. Linear post-transition kinetics of mass gain is therefore applied here starting from the transition point, which is known from the fitting to experimental data.

This approach is kept as simple as possible, to allow easy treatment of temperature transient experiments, and a general application of the demonstration version. As first parameter $K_p(T)$, the already known parabolic rate coefficient of mass gain, is introduced. This function is sufficient to describe the mass gain kinetics in the whole field of “normal oxidation” up to the criterion $a_1(T)$ (a for alternation), a “critical” mass gain. Within the “pre-transition” field, starting from $a_1(T)$ an unknown cubic rate coefficient $K_c(T)$ shall be valid (index c for cubic). Two conditions are used to couple both fields strictly: At $a_1(T)$ continuity of curve and slope for the two branches, the parabolic and the cubic, is required. According to a simple calculation, those two conditions define the following relation between both rate coefficients:

$$K_c = 3/2 \cdot K_p \cdot a_1 \qquad [mg^3*dm^{-6}*s^{-1}] \tag{1}$$

The relation is interpreted as the full determination of $K_c(T)$, provided that $a_1(T)$ is known. So it can be avoided to introduce an additional and moreover arbitrary kinetic parameter, In this sense it is preferred to use the known parameter $K_p(T)$ indirectly for the pre-transition oxidation as well.

The next task is to couple the pre-transition field to the post-transition range. The interface between both fields, as defined by experimental results is the point of rate transition in temperature dependence. The respective function $a_2(T)$ is introduced for the calculation. A steady kinetic curve, but a change in slope at the transition point is defined according to idealized experimental findings. Consequently, only one continuity condition is utilized, whereas the slope of the post transition rate equation remains as free option. A linear time dependence of the post-transition rate law is chosen.

As default option the rate coefficient $K_l(T)$ shall be equal to the average within the pre-transition period, or more generally, equal to its virtual isothermal correspondence in the temperature transient case. The latter definition allows to abstract from the use of “critical” oxidation time values and to prefer “critical” mass gain values, here $a_1(T)$ and $a_2(T)$. Omitting the straightforward calculation, the relation for the post-transition rate law is given:

$$K_l = 3 \cdot K_p \cdot \frac{a_1 \cdot a_2}{a_1^3 + 2 \cdot a_2^3} \qquad [mg*dm^{-2}*s^{-1}] \qquad (2)$$

Again for this relation, the rate coefficient, here $K_l(T)$, can be seen as fully determined, provided that $a_1(T)$ and $a_2(T)$ are known. Up to now, no real materials data were necessary. On the one hand, the procedure suggests to attribute all kinetic aspects to the given parabolic rate law $K_p(T)$ and the closely linked cubic and linear rates, which are only indirectly utilized. On the other hand, the field of breakaway-related kinetic consequences is defined by the critical values $a_1(T)$ and $a_2(T)$, which are only artificial mathematical functions as long as they are not determined through a fitting process. Even after that, the question remains open, whether $a_1(T)$ is a physically justified and sufficiently reasonable parameter, really corresponding to the oxide phase transformation mechanisms.

3.2 Calculation method

Calculations were run by PC and applying SigmaPlot®, ©SPSS Inc., for demonstration of feasibility. The numerical procedures were given as so-called “user defined transforms”. Work sheet presentation, plotting tools, and statistics aids for curve fitting were utilized. In the application to experiments, using real materials data and the resulting values of the fitting, the start data (t=0) T_0, m_0, are given, and the steps in t and T are chosen. The correct choice of the offered parabolic, cubic, or linear rate law of mass gain increment is automatically found in the program according to the given criteria a_1 and a_2 before each new time step. Runs in the form of rising and falling linear temperature ramps as well as isothermal holding periods between ramps have confirmed the consistency of the program. At first, isothermal runs were repeated with modified parameter $a_1(T_i)$ to get best fit of $a_2(T_i)$ to a set of experimental data for several temperatures T_i for which reliable experimental results were available.

3.3 Data input and fitting

In the evaluation method the parabolic rate coefficient of mass gain according to Leistikow [Leis1978, Leis1983] is applied.

$$K_p = K_p^{Lei} = 5.2418 \cdot 10^9 \cdot \exp(-20962/T) \qquad [mg^2*dm^{-4}*s^{-1}] \qquad (3)$$

This correlation is quite comparable to the often favored Cathcart-Pawel correlation [Cath1977]. But nevertheless one has to keep in mind that the regime boundary criteria $a_1(T)$ and $a_2(T)$, which will be determined later, are fully consistent with this correlation choice only. In other words, applying the procedure to the Cathcart-Pawel correlation would result in some deviation of the criteria values. An expanded range of validity of those rate correlations can be expected within the whole regime of normal oxidation as consequence of the extension of the t-ZrO_2 stability field to the lower temperatures.

But a contribution to uncertainty follows from the application of the respective correlation as extrapolated below the temperature range of its validation data base (1273-1773 K). No other correlation is needed as data input for the description of the cubic and the linear regime, since the pre-transition and the post-transition rates are indirectly given (see relations (1) and (2), previous chapter) as soon as the regime boundary criteria $a_1(T)$ and $a_2(T)$ are known.

Determination of $a_2(T)$: Experimental mass gain and scale growth data from a comprehensive set of isothermal experiments [Leis1983] were used. Accordingly, no breakaway transition occurs at 1373 K and above. From 1323 K to the lowest covered temperature 873 K breakaway-related behavior can be realized: Below and above the (α+β)-Zr duplex phase stability of the Zry-4 matrix, i.e. 1093 to 1243 K rather abrupt mass gain rate changes with time allowed the definition of idealized transition points for the respective test temperatures. Within the duplex phase range, i.e. for test temperatures 1123, 1173, and 1223 K the inspection of test sample cross section micrographs revealed those exposure durations leading to first signs of oxide pustules growth. In total, ten respective mass gain / time data points were extracted from the experimental results and interpreted as cub./lin. transition data points $a_2(T_i)$. Curve fitting to an exponential temperature dependence of transition mass gain, the parameter $a_2(T)$ in the calculation procedure, was satisfactory: All data points were within the 95% confidence range, and the statistic value R-squared was above 0.99.

Determination of $a_1(T)$: A series of isothermal pre-calculations was run, in which the arbitrary initial value for $a_1(T_i)$ was adapted for step-wise improved $a_2(T_i)$ fit of the calculation. For example a still too large $a_1(T_i)$ value corresponded to an over-predicted $a_2(T_i)$ value and required earlier curve downward bending via a reduced $a_1(T_i)$ value to improve the matching. The post-transition phase was suppressed in the fitting pre-calculations for undisturbed comparison with the experimentally known transition points. This procedure of adapting the calculation to the experimental transition point data $a_2(T_i)$ was repeated for the partial data sets in the temperature range 873 to 1373 K in order to obtain the $a_1(T_i)$ values. Adaptation of an $a_1(T)$ curve of exponential type to the $a_1(T_i)$ data was possible with similar statistic significance as for $a_2(T)$.

3.4 Results

As explained earlier the determination of $a_2(T)$ is to be seen as the evaluation of experimental results [Leis1983]. An exponential dependence on temperature with three coefficients was gained:

$$\boldsymbol{a}_2(\boldsymbol{T}) = 4.828 \cdot 10^{1} + 5.529 \cdot 10^{-3} \cdot \exp(9.383 \cdot 10^{-3} \cdot \boldsymbol{T}) \quad [\text{mg*dm}^{-2}] \qquad (4)$$

The a_1 values for the different test temperatures, optimized in pre-calculation sets as previously described, allowed curve fitting to another exponential temperature dependent function with three coefficients:

$$\boldsymbol{a}_1(\boldsymbol{T}) = 2.24 \cdot 10^{1} + 1.03 \cdot 10^{-7} \cdot \exp(1.769 \cdot 10^{-2} \cdot \boldsymbol{T}) \quad [\text{mg*dm}^{-2}] \qquad (5)$$

The knowledge of both functions completes the mathematical formalism, so that checking for consistency with available isothermal experimental results can follow. Moreover, since the procedure is also ready for transient calculations, some consequences of application to transient cases shall be described and discussed as well.

Fig. 1 is to illustrate the field of temperature dependent mass gain. During an isothermal steam exposure a Zry-4 specimen moves horizontally from left to right. The curves a_1 and a_2 divide the field into three regimes, the parabolic, the cubic, and the linear one. The crossing of the a_1 and a_2 curves is registered at 1313 K. This temperature is to be compared to the experimental observation of a breakaway transition up to 1323 K, and the absence of the effect at 1373 K and above. Up to 1313 K a regime of cubic pre-transition kinetics is predicted. According to the definition within the formalism, a_1 should be the first and a_2 the second criterion of alternation of the kinetics in the course of the oxidation. Consequently, the a_1 segment beyond and above the crossing point makes no physical sense. The respective a_2 segment, however, allows two interpretations. According to a simple base case option the a_2 branch above the crossing point shall be interpreted as non-physical so that the breakaway phenomena are predicted to disappear at 1313 K. However, this option couples the breakaway transition perhaps unduly strong to the occurrence of a pre-transition regime with cubic kinetics. According to an alternative interpretation option a direct transition from parabolic to linear kinetics has been included in the formalism to be prepared for more experiment-oriented calculations in the higher temperature range. Following the available experimental results more strictly, the a_2 line is truncated in the middle between 1323 and 1373 K, i.e. at 1348 K. Using this option the analytical description can be adapted closer to the experimental results for 1323 K. Horizontal temperature limit lines at 1348 and 1313 K, as used for this and the base case option, respectively, are not included in Fig. 1, to let the choice between the options open. More precisely dedicated future experimental results should decide this item of the analytical description.

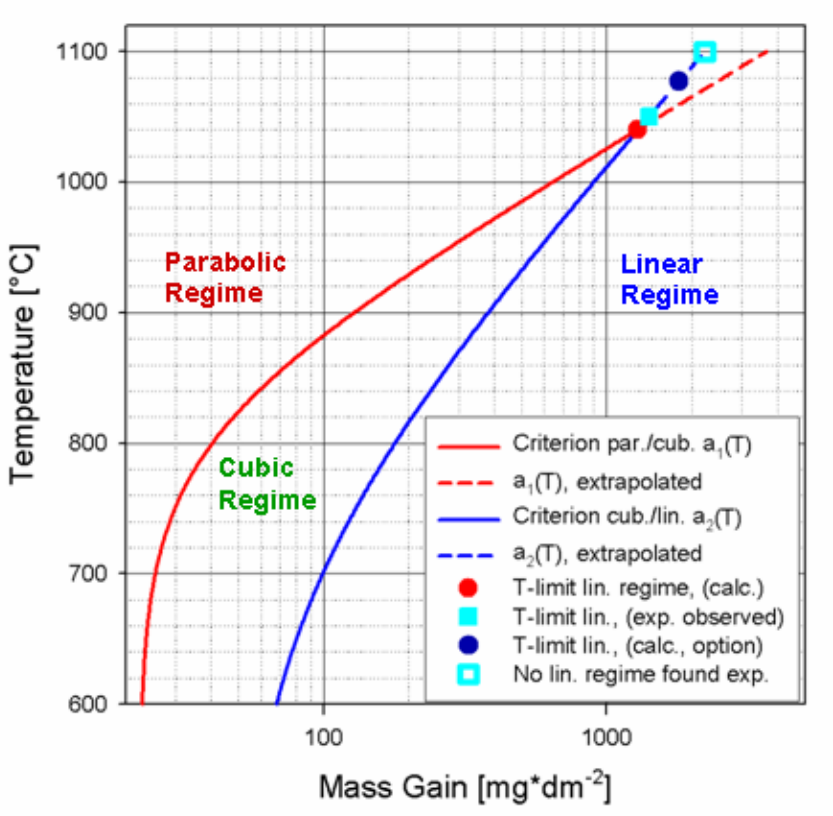

Fig. 1: Boundaries of the kinetic regimes within the temperature vs. mass gain field, determined in the fitting procedure

Fig. 2 compares a partial set of experimental results on Zry-4/steam oxidation kinetics (data points from [Leis1983]) with calculations in the temperature range 1373 to 1173 K in a double logarithmic representation of mass gain vs. time of exposure. One can realize that the calculation scheme represents automatically the crossing of the curves for 1373 and 1273 K as result of the transition regime limit in between. Since the depicted partial data set did not include experiments at 1323 K, the detailed differences between the above described analytical options shall not be repeated here. In general, a satisfactory adaptation to the experimental facts has been gained. It is mentioned that the chosen option for the post-transition rate seems acceptable as well. For all temperatures in the range the calculations resulted in a fair representation of the real transition points. But, as expected, the special behavior of specimens with (α+β)-Zr duplex phase matrix, here 1223 and 1173 K, is not verified. The sluggish kinetic change as result of the localized transition onset, corresponding to the oxide pustules growth, is not treated in the actual version of the calculation scheme, and this explains the increase of over-prediction with time in the post-transition range.

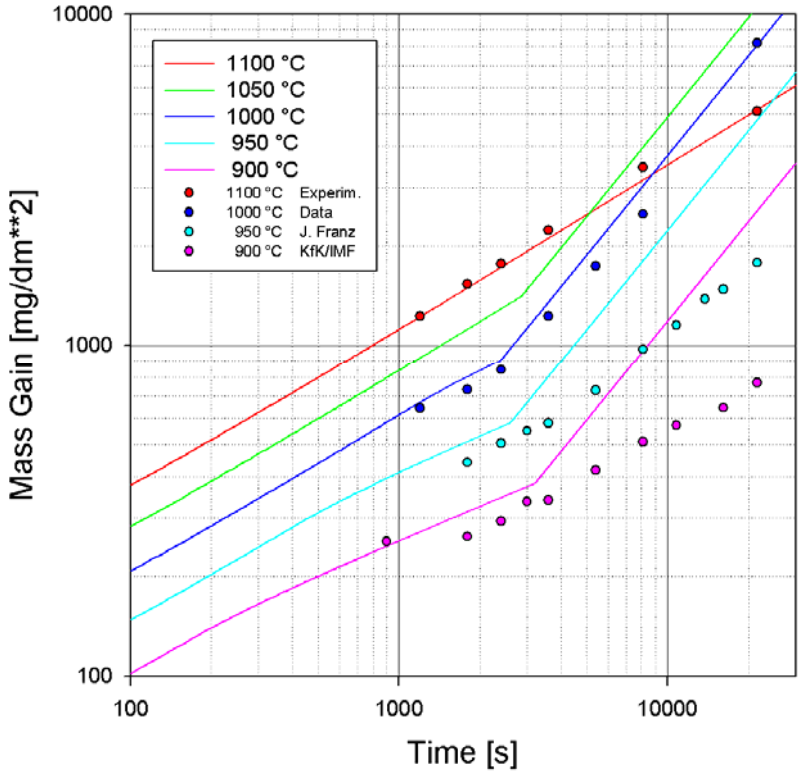

Fig. 2: Comparison of mass gain vs. time between a partial set of experiments (data points unpublished results included in [Leis1983]) and calculations (curves) for the temperature range 1373 to 1173 K

At lower temperatures an again improved match of the kinetics is registered.

Fig. 3 compares the set of experimental results (data points) gained in the temperature range 1123 to 873 K with respective calculation results (curves). For 1123 K the good curve fit to the pre-transition data is in contrast to the much exaggerated post-transition rate compared to the real one, but this expected deviation seems to confirm the given interpretation as due to the pustular scale growth effect, which is not covered here. Good fit up to the transition is registered for all other temperatures in the range, as well as a fair prediction of the transition points. The calculated post-transition rates seem to average the rate variations along the sequence of experimental post-transition results. The considerable scatter of the experimental post-transition data can be related to a kind of periodicity in the sense of post-transition cycles observed for the breakaway type variant mentioned by Cox [Cox2005]. In contrast, the calculation combines the extremes of assuming on the one hand scale protection loss coupled for the whole specimen and on the other hand a time averaged post-transition oxidation rate, so that a distinct transition point is created but post-transition cycles are suppressed. Within those simplifications the analytical description of the real materials behavior can be hardly improved.

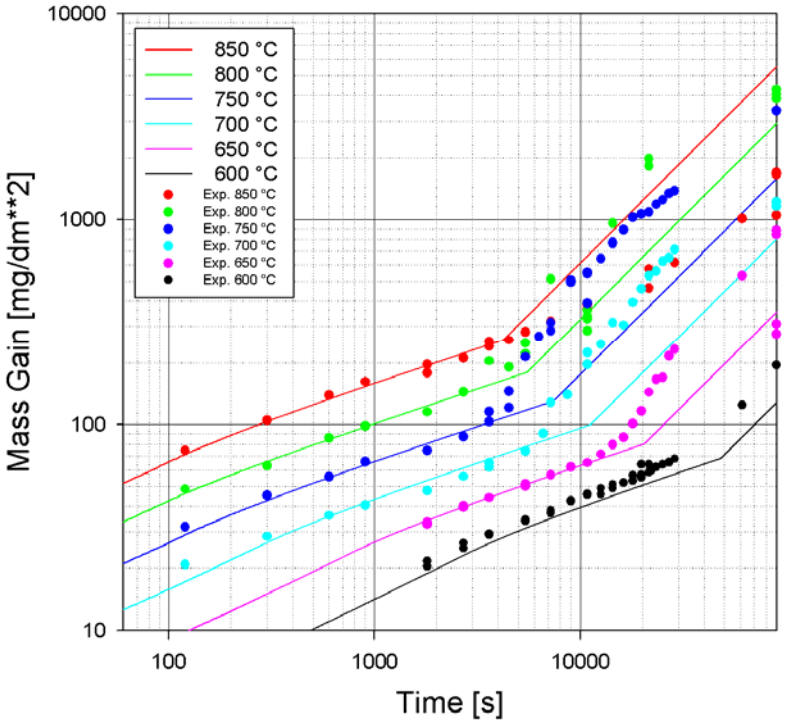

Fig. 3: Comparison of mass gain vs. time between a set of experiments (data points [Leis1983]) and calculations (curves) for the temperature range 1123 to 873 K

The following two figures extrapolate the application of the calculation method to temperatures below the range of data used for its adaptation. The calculated curves are compared to correlations, formulated by the given authors to represent the results of autoclave experiments on the Zry-4/water oxidation kinetics. As mentioned in Chap. 2, those correlations have served for comparison with in-pile oxidation results in a review report by Garzarolli et al. [Garz1980].

One difference, illustrated in **Fig. 4** between the empirical correlations from the literature and the here described calculation results is related to the assumed cubic pre-transition kinetics in those compared to the change from parabolic to cubic, as treated here. The deviations of the critical mass gains are smaller than those of the transition times for both temperatures, referring to the correlations, which represent the experimental results. Accordingly, the representation of those data is worsened and non-conservative with the presented approach. On the other hand, no large error due to the extrapolation of the high-temperature fit to the considered temperature regime has to be registered, a fact supporting the reliability of the K_p^{Lei} rate correlation [Leis1978 and Leis1983] as well as the pre-transition treatment.

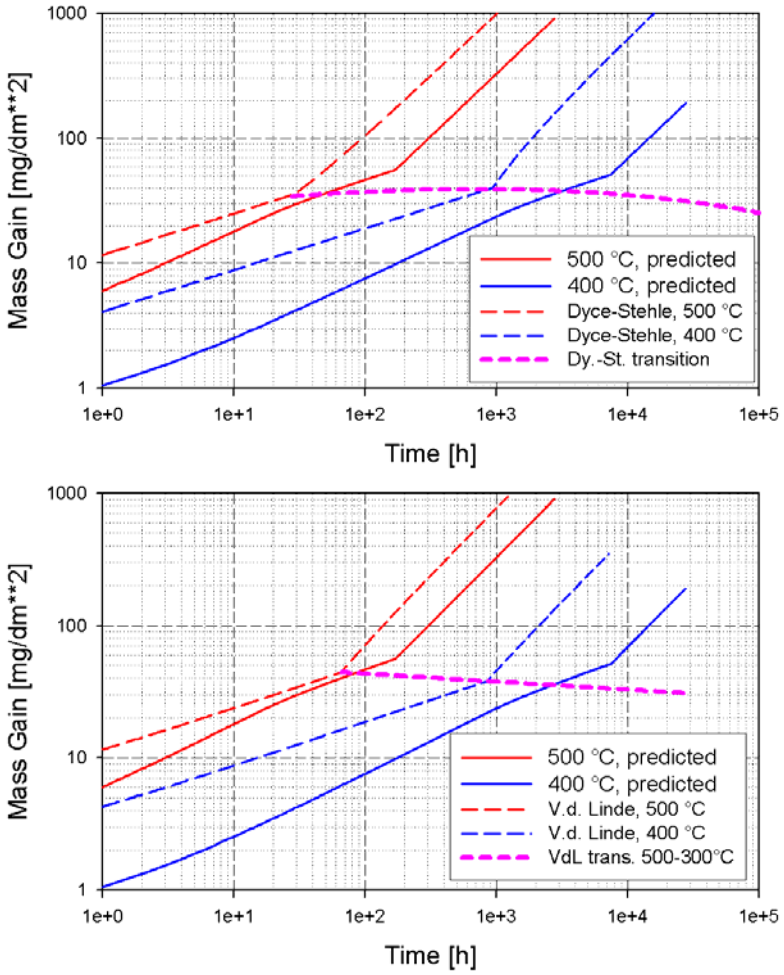

Fig. 4: Comparison of the correlations according to Dyce-Stehle and Van der Linde for the description of autoclave test results (dashed correlations and transition boundary lines as cited in [Garz1980]) with calculated results (full lines)

In **Fig. 5** the Hillner correlation set is shown for 673 K only, the upper limit of validity, and in comparison to the calculation similar deviations are registered as discussed above for the two other correlation sets. The Dalgaard post transition correlation (no pre-transition line defined) is verified for 773 K, whereas its temperature dependence is much less compared to the other correlations and the calculation as well.

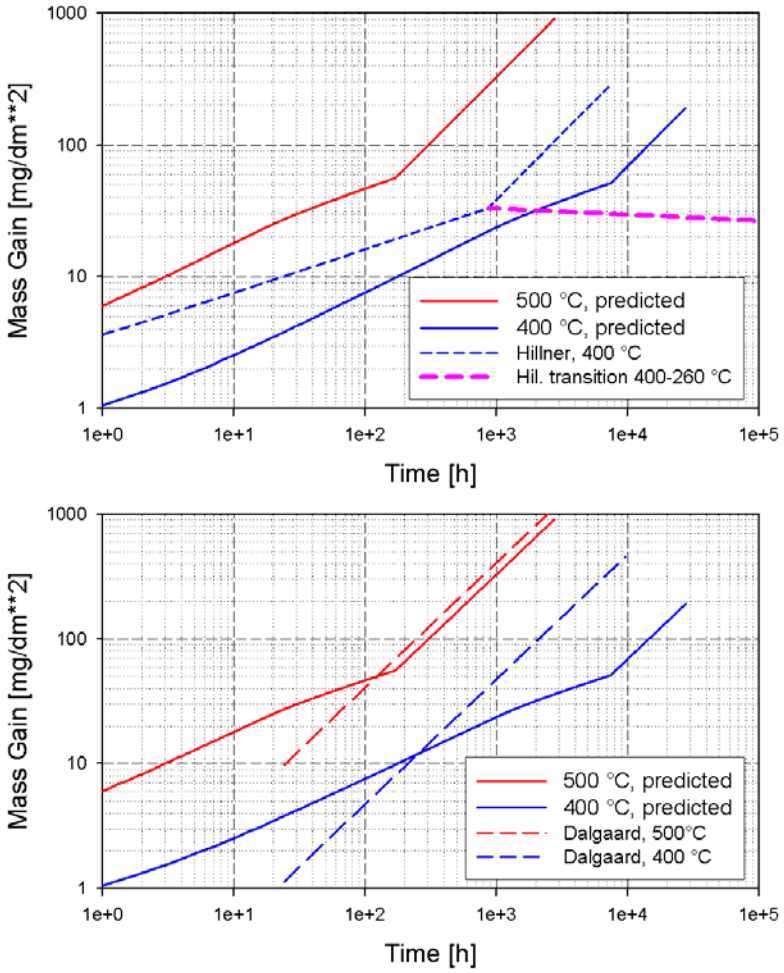

Fig. 5: Comparison of the correlations according to Hillner and Dalgaard for the description of autoclave test results (dashed correlations and transition boundary line as cited in [Garz1980]) with calculated results (full lines)

Without illustration it is further mentioned, that investigations towards advanced zirconium alloys for application under supercritical water reactor conditions are presently performed [Mot2006]. The recently given information seems to indicate, that the oxidation resistance of candidate alloys is comparable to Zry-4 in the (short term) range of “normal oxidation”, whereas a pronounced retardation of the breakaway transition as function of the alloy composition has been demonstrated. It may be helpful to consider the unchanged application of the here described novel calculation procedure for cross comparison with experimental results on advanced cladding materials and in alloy development.

The consistency of the calculation procedure during temperature changes has been checked on basis of simulation runs composed of a linear heat-up ramp, a holding period, and a linear cool-down segment.

Fig. 6 shows the development of mass gain together with the temperature cycle for three calculations with different holding temperatures close to the temperature limits of the breakaway regime. In the worksheet, the SigmaPlot® transform allowed to calculate the temperature step for each time step, to verify the altered $a_1(T)$ and $a_2(T)$ criteria values, and to calculate the mass gain increment accordingly. During the common upward ramp the identical change from parabolic to cubic and back to the parabolic rate law is marked for the three runs. Those automatic actions are adequate, because the increasing mass gain is mostly compensated by the increase of the $a_1(T)$ value for the special temperature increase rate of the given ramp. On the blue curve the second entrance into the cubic pre-transition regime during the holding period, and the transition point initiating enhanced mass increase rate are indicated. On the green curve the parabolic to linear transition during the holding above the cubic regime is indicated, after which the mass gain is switched to post-transition kinetics. A test specimen according to the curve in red would have spent the holding period above the breakaway regime and shows the comparatively lowest mass gain. It enters into the post-transition field soon after cool-down initiation, but during this period all curves show not much additional mass gain.

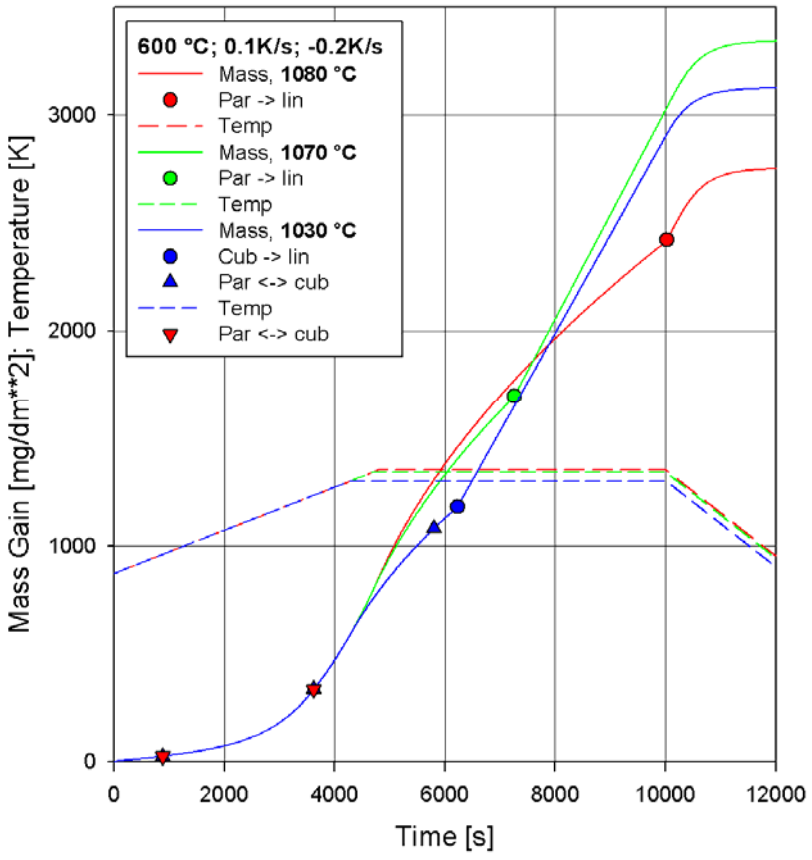

Fig. 6: Verification of the consistent calculation of mass gain progress during the temperature-transient phases of three idealized exposure temperature histories, remaining below or passing beyond breakaway regime temperature limits, respectively

3.5 Discussion

With the presented evaluation method a satisfactory fit to experimental data in a large temperature range has been demonstrated. A reasonable correspondence was gained across the whole field of oxidation durations and temperatures without changing formalism and parameters. This is a strong argument in support of the parabolic rate correlation for mass gain according to Leistikow [Leis1978 and Leis1983], its extrapolation to lower temperatures, as well as the determined limit $a_1(T)$, introduced as semi-mechanistic parameter for the separation of the parabolic from a cubic regime. Nevertheless, caution is indicated if this parameter should be more closely compared to mechanistic results on oxide phase transformation studies, since various errors might have compensated each other. On the other hand, the main purpose of the report is to offer the approach in simple form in order to facilitate its unchanged use for comparison purposes as Zry.-4 / steam reference.

Some refinement of the evaluation procedure would be possible. More detailed investigation of the temperature limit of breakaway behavior has been mentioned as experimental task, whereas the described analytical option of direct par./lin. transition is available and already checked for consistency. The deviation of the calculated post-transition kinetics from the experimentally observed oxide pustules growth and related sluggish post-transition mass gain within the (α+β)-Zr) temperature range arises as further anomaly, deserving special mainly experimental effort, because not all aspects are clear. Since the effect does not seem to occur in the systems Zr/oxygen and Zr/air, some influence of hydrogen, released from steam consumption might play a role besides that of the duplex phase matrix. The post-transition treatment is open for alternative options of linear rate definition or the simulation in total. The given temperature functions for $a_1(T)$ and $a_2(T)$ are not claimed to be defined to absolute precision. A refined adaptation of the $a_2(T)$ criterion to other experimental data is quite simple, of course the $a_1(T)$ parameter would depend on that. Such an effort would be also necessary if the Cathcart-Pawel correlation [Cath1977] should be preferred. The application of the procedure to experimental series performed in other oxidizing media should be helpful and would be of general interest as well.

Links between steam, pressurized water, and power plant media have been illustrated, and the presently established strict distinction between the treatment of Zry-4 oxidation at high accident temperatures and that of the corrosion at normal operation temperatures can be discussed and put into question. It is not intended to propose the replacement of empirical correlations established for investigations in the service temperature range by use of the here developed analytical scheme. Nevertheless, an advantage of the offered novel approach is seen in the continuity within the whole temperature field on basis of an established single parabolic rate law correlation. Embedded therein, a simplified treatment of the breakaway related kinetic consequences is given, which aims at linking those to involved physical parameters.

The main benefit of the approach is seen in the flexibility of the de-coupled treatment of kinetics and regime boundary data. Its adaptation to the treatment of other zirconium alloys and oxidizing media requires comparably broad and reliable bases of experimental data. The message in this respect is, that the basic behavior is expected to be similar, despite large specific differences, which are not yet completely understood.

4 References

[Ahm1975] T. Ahmed, L.H. Keys, The Breakaway Oxidation of Zirconium and its Alloys; A Review", J. Less Common Metals, 39 (1975) 99

[ANS2004] American Nuclear Society, Proceedings of the 2004 Int. Meet. on LWR Fuel Performance, Sept. 19-22, Orlando, FL, USA

[Barb1995] P. Barberis, "Zirconia powders and Zircaloy oxide films: tetragonal phase evolution during 400 °C autoclave tests", J. Nucl. Mater. 226 (1995) 34-43

[Cath1977] J.V. Cathcart et al.: Zirconium Metal-Water Oxidation Kinetics; IV. Reaction Rate Studies. ORNL/NUREG-17, 1977

[Cox1976] B. Cox, "Towards an Understanding of Zirconium Alloy Corrosion", on the occasion of the William J. Kroll Medal Presentation, Quebec City, Aug. 11, 1976, AECL-5548

[Cox2005] B. Cox, "Some thoughts on the Mechanisms of In-Reactor Corrosion of Zirconium Alloys", J. Nucl. Mater. 336 (2005) 331-368

[Garz1980] F. Garzarolli, D. Jorde, R. Manzel, G.W. Parry, P.G. Smerd; "Review of PWR Fuel Rod Waterside Corrosion Behavior", EPRI NP-1472, 1980

[Godl1991] J. Godlewski, J.P. Gros, M. Lambertin, J.F.Wadier, H. Weidinger, ASTM-STP 1132 (1991) 416

[Godl1994] J. Godlewski, ASTM-STP 1245 (1994) 663

[Godl2000] J. Godlewski, P. Bouvier, G. Lucazeau, L. Fayette, ASTM STP 1354 (2000) 877

[Kim1990] D.J. Kim, J. Am. Ceram. Soc. 73 (1990) 115

[Leis1978] S. Leistikow, G. Schanz, H. v. Berg: Kinetik und Morphologie der isothermen Dampf-Oxidation von Zircaloy 4 bei 700-1300 °C. KfK2587, 1978

[Leis1983] S. Leistikow, G. Schanz, H. v. Berg, A.E. Aly, "Comprehensive Presentation of Extended Zircaloy-4/Steam Oxidation Results (600-1600 °C)", OECD-NEA-CSNI/IAEA Specialists' Meeting on Water Reactor Safety and Fission Product Release in Off-Normal and Accident Conditions; Risø Nat. Lab., Denmark, May 16-20,1983, Proc. IAEA IWGFPT/16, 188-199

[Leis1985] S. Leistikow, G. Schanz, "The Oxidation Behavior of Zircaloy-4 in Steam between 600 and 1600 °C", Werkstoffe und Korrosion 36, (1985) 105

[Li1994] P. Li, I.W. Chen, J.E. Penner-Hahn, J. Am. Ceram. Soc. 77 [1994] 1281

[Mot2006] A. Motta et al.: Zirconium Alloys for Supercritical Water Reactor Applications: Challenges and Possibilities. ANS Annual Meeting, Reno (NV), June 4-8 2006; American Nuclear Society Transactions Vol. 94

[Naka1967] T. Nakayama, T. Koizumi, “On the Polymorphic Transformation of Zirconium Dioxide Associated with the Breakaway During High Temperature Oxidation of Zr and Some Zr Alloys”, J. Japan Inst. Metals 31 (7), July 1967, 839-845 (Jap.); Nuclear Science Abstracts of Japan No. 05468; NSJ-Tr-No. 138, Sept. 1968

[Park2004] J.-Y. Park, H.-G. Kim, Y.H. Jeong, Y.-H. Jung, “Crystal Structure and Grain Size of Zr Oxide Characterized by Synchrotron Radiation Microdiffraction”, J. Nucl. Mater. 335 (2004) 433-442

[Paw1977] R.E. Pawel, J.V. Cathcart, J.J. Campbell, S.H. Juri, Zirconium Metal-Water Oxidation Kinetics V. Oxidation of Zircaloy in High Pressure Steam, ORNL/NUREG-31, 1977

[Roy1970] C. Roy, G. David, J. Nucl. Mater. 37 (1970) 71

[Sabo1975] G.P. Sabol, S.B. Dalgaard, J. Electrochem. Soc. 122 (1975) 316

[Sawa1977] A. Sawatzki, G.A. Ledoux, S. Jones, “Oxidation of Zirconium During a High-Temperature Transient”, ASTM Special Technical Publication STP 633, 1977

[Sch1981] G. Schanz, S. Leistikow, “Microstructural Reasons for Mechanical Oxide Degradation (Breakaway Effect) and Resulting Kinetical Anomalies of Zircaloy 4/Steam High-Temperature Oxidation”, 8th Int. Congress on Metallic Corrosion, Mainz, Germany, Sept. 6-11, 1981, Proc. DECHEMA, Vol. II, [1981) 1712-1717

[Scha1981] G. Schanz, S. Leistikow, ZrO_2-Scale Degradation During Zircaloy-4 High Temperature Steam Exposure; Microstructural Mechanisms and Consequences for PWR Safety Analysis, ANS/ENS Top. Meeting on Reactor Safety Aspects of Fuel Behaviour, Aug. 2-6, 1981, Sun Valley, ID, USA, Proc. Vol. II, p. 342

[Scha2003] G. Schanz, “Recommendations and Supporting Information on the Choice of Zirconium Oxidation Models in Severe Accident Codes”, Forschungszentrum Karlsruhe, FZKA 6827, 2003

[Scha2006] G. Schanz: Semi-mechanistic Approach for Evaluation of Zr Oxidation Experiments. ANS Annual Meeting, Reno (NV), June 4-8 2006; American Nuclear Society Transactions Vol. 94

[Vesh1997] A.V. Berdyshev, L.V. Matveev, M.S. Veshchunov, “Development of the Data Base for the Kinetic Model of the Zircaloy 4/Steam Oxidation at High Temperatures (1000 °C $\leq$ T $\leq$ 1825 °C), Russian Academy of Sciences, Nuclear Safety Institute, IBRAE-97-05, 1997

[Vol2004] A. Volchek et al., “Advanced treatment of zircaloy cladding high-temperature oxidation in severe accident code calculations, Part I. Experimental database and basic modeling, Part II. Best-fitted parabolic correlations, Part III. Verification against representative transient tests”, Nucl. Eng. Des. 232 (2004) 75-109

[Yilm2006] A. Yilmazbayhan, E. Breval, A.T. Motta, R.J. Comstock; “Transmission electron microscopy examination of oxide layers formed on Zr alloys”, J. Nucl. Mater. 349 (2006) 265-281

Annex A : Examples of the developed SigmaPlot®, ©SPSS Inc. user-defined transforms

One convention for SigmaPlot®, ©SPSS Inc. user-defined transforms is that lines, giving comments, have to be set between semicolons. In the definition of variables, which is to be done first, all combinations of letters and numbers are allowed that do not interfere with given names for commands.

Scheme of isothermal pre-calculations with arbitrary a_1 and a_2 values and reaction rate data.

```
T-Iso.xfm
jsv5D.,
cell(2,1)=1
n=3000
a1=20
a2=50
;a are the critical mass gains for rate law change initiation;
q1=2
; parab. x**2=q1*t;
q2=60
; kub. x**3=q2*t;
q3=0.2
;lin. X=q3*t;
col(1)=data(0,n,1)
cell(3,1)=q1/(2*cell(2,1))
; dpx;
cell(4,1)=q2/(3*cell(2,1)**2)
; dcx;
cell(5,1)=q3
; dlx;
for i=2 to 3001 step 1 do

  if round(cell(2,i-1),2)<a1 then
  cell(2,i)=cell(2,i-1)+cell(3,i-1)
  end if
  if round(cell(2,i-1),2)>=a1
  and round(cell(2,i-1),2)<=a2 then
  cell(2,i)=cell(2,i-1)+cell(4,i-1)
  end if
  if round(cell(2,i-1),2)>a2 then
  cell(2,i)=cell(2,i-1)+cell(5,i-1)
  end if
cell(3,i)=q1/(2*cell(2,i))
cell(4,i)=q2/(3*cell(2,i)**2)
cell(5,i)=q3
end for
```

Check for fitting of experimental transition mass gain a_2 results to an exponential temperature function with three coefficients. The data for 500 °C and below are excluded here.

```
T-Fit Mass a2.xfm
jsv5D.,
x=data(0,1400,1)
col(1)=x
;cell(2,624)=28.9;
;cell(2,674)=30.4;
;cell(2,724)=33.7;
;cell(2,774)=39.2;
cell(2,874)=65.0
cell(2,974)=102.6
cell(2,1074)=183.5
cell(2,1174)=372.8
cell(2,1274)=903.7
cell(2,1351)=1800
b=9.383*10**-3
a=5.529*10**-3
y0=48.28
y=y0+a*exp(b*x)
put y into col(3)
```

Check for fitting of experimental transition mass gain a_2 results to an exponential temperature function. Data for all temperatures are used.

```
T-Fit a2.xfm
jsv5D.,
x=data(0,1400,1)
col(1)=x
cell(2,624)=28.9
cell(2,674)=30.4
cell(2,724)=33.7
cell(2,774)=39.2
cell(2,874)=65.0
cell(2,974)=102.6
cell(2,1074)=183.5
cell(2,1174)=372.8
cell(2,1274)=903.7-0.02*cell(1,1274)
cell(2,1324)=1800-0.02*cell(1,1324)
b=1.162*10**-2
a=3.641*10**-4
y=0.02*x+a*exp(b*x)
put y into col(3)
```

Check for fitting of a_1 iteration results to an exponential temperature function

```
T-Fit Mass a1.xfm
jsv5D.,
;a2 values acc. to Eva Fit Mass a2.xfm;
;iteration gives a1 for 600-1000 °C;
```

```
;a1 function w/o 600 °C value;
x=data(0,1400,1)
col(1)=x
cell(2,874)=41.74
cell(2,974)=25.20
cell(2,1074)=40.76
cell(2,1174)=127.5
cell(2,1274)=639
b=1.769*10**-2
a=1.03*10**-7
y0=2.24*10**1
y=y0+a*exp(b*x)
put y into col(3)
```

Sensitivity check for fitting of a_1 iteration results to changes of temperature function

```
T-Fit a1.xfm
jsv5D.,
x=data(0,1400,1)
col(1)=x
cell(2,874)=23.6
cell(2,974)=26.3
cell(2,1074)=55.6
cell(2,1174)=172
cell(2,1274)=738
b=1.557*10**-2
a=1.768*10**-6
y0=2.166*10**1
y=y0+a*exp(b*x)
put y into col(3)
```

Transform for isothermal calculation at 773 K

```
T-Iso500.xfm
jsv5D.,
;T-Iso500C;
;transform structure for isoth case;
;T<=1348K;
;col(1)=t in sec;
;cells(2,1 2 3) = T a1 a2;
;cells(2, 4 5 6) = q1 q2 q3;
;column 7 id for par cub lin 1 2 3;
dt=360
n=10**7
t=data(0,n,dt)
T=773
a1=22.4+1.03*10**-7*exp(0.01769*T)
a2=48.28+0.005529*exp(0.009383*T)
kuh=20962
q1=5.2418*10**9*exp(-kuh/T)
q2=3/2*a1*q1
q3=3*q1*a1*a2/(a1**3+2*a2**3)
put t into col(1)
```

```
cell(2,1)=T
cell(2,2)=a1
cell(2,3)=a2
cell(2,4)=q1
cell(2,5)=q2
cell(2,6)=q3

cell(3,1)=1.5
;(start value for mass);
cell(4,1)=cell(2,4)/2*dt/cell(3,1)
;(start incr for par case);
cell(5,1)=cell(2,5)/3*dt/cell(3,1)**2
;(start incr for cub case);
cell(6,1)=cell(2,6)*dt
;(start incr for lin case);
;next task: case definition;

for i=2 to (n/dt)+1 do

  if cell(3,i-1)<a1 then
  cell(3,i)=cell(3,i-1)+cell(4,i-1)
  cell(7,i)=1
  end if

  if cell(3,i-1)>=a1 and cell(3,i-1)<a2 then
  cell(3,i)=cell(3,i-1)+cell(5,i-1)
  cell(7,i)=2
  end if

  if cell(3,i-1)>=a2 then
  cell(3,i)=cell(3,i-1)+cell(6,i-1)
  cell(7,i)=3
  end if

  cell(4,i)=q1/2*dt/cell(3,i)
  cell(5,i)=q2/3*dt/cell(3,i)**2
  cell(6,i)=q3*dt
;instead cell(2,4 5 6) alternatively q123;
end for

col(8)=col(1)/3600
;col(8)=t in hrs;
```

Transform for isothermal calculation at 673 K in a worksheet together with the previous example

```
T-Iso400.xfm
jsv5D.,
;T-Iso400C;
;transform structure for isoth case;
;T<=1348K;
;col(9)=t in sec;
;cells(10,1 2 3) = T a1 a2;
```

```
;cells(10, 4 5 6) = q1 q2 q3;
;column 15 id for par cub lin 1 2 3;
dt=3600
n=10**8
t=data(0,n,dt)
T=673
a1=22.4+1.03*10**-7*exp(0.01769*T)
a2=48.28+0.005529*exp(0.009383*T)
kuh=20962
q1=5.2418*10**9*exp(-kuh/T)
q2=3/2*a1*q1
q3=3*q1*a1*a2/(a1**3+2*a2**3)
put t into col(9)
cell(10,1)=T
cell(10,2)=a1
cell(10,3)=a2
cell(10,4)=q1
cell(10,5)=q2
cell(10,6)=q3

cell(11,1)=0.5
;(start value for mass);
cell(12,1)=cell(10,4)/2*dt/cell(11,1)
;(start incr for par case);
cell(13,1)=cell(10,5)/3*dt/cell(11,1)**2
;(start incr for cub case);
cell(14,1)=cell(10,6)*dt
;(start incr for lin case);
;next task: case definition;

for i=2 to (n/dt)+1 do

  if cell(11,i-1)<a1 then
  cell(11,i)=cell(11,i-1)+cell(12,i-1)
  cell(15,i)=1
  end if

  if cell(11,i-1)>=a1 and cell(11,i-1)<a2 then
  cell(11,i)=cell(11,i-1)+cell(13,i-1)
  cell(15,i)=2
  end if

  if cell(11,i-1)>=a2 then
  cell(11,i)=cell(11,i-1)+cell(14,i-1)
  cell(15,i)=3
  end if

  cell(12,i)=q1/2*dt/cell(11,i)
  cell(13,i)=q2/3*dt/cell(11,i)**2
  cell(14,i)=q3*dt
;instead cell(10,4 5 6) alternatively q123;
end for

col(16)=col(9)/3600
;col(16)=t in hrs;
```

Calculation of idealized temperature transients, composed of a linear heat-up ramp, a holding period and a cool-down ramp.

```
T-MassWallRanges.xfm
jsv5D.,
;Leistikow-correlation;
;a1 und a2 are functions of T;
;Sources of a1, a2: T-Fit Mass ai.xfm;
;Parabolic for T>1350 K;
;Parabolic for masses<a1 and <a2 to 1350 K;
;Cubic for masses from a1 to <a2 and up to 1350 K;
;Linear for masses from a2 and up to 1350 K;
;Column 12: Range control indicator No. 1 to 3 (par. -  lin.);
;Column 2: T-ramp up, holding, down;
dt=10
n=12000
t=data(0,n,dt)
put t into col(1)
a=873
b=0.1
c=0.2
put a into cell(2,1)
for j=2 to n/dt+1 step 1 do
if cell(1,j)<=4800 then
cell(2,j)=cell(2,j-1)+b*dt
end if
if cell(1,j)>4800 and cell(1,j)<=10000 then
cell(2,j)=cell(2,j-1)
end if
if cell(1,j)>10000 then
cell(2,j)=cell(2,j-1)-c*dt
end if
end for
a1=22.4+1.03*10**-7*exp(0.01769*col(2))
a2=48.28+0.005529*exp(0.009383*col(2))
kuh=20962
q1=5.2418*10**9*exp(-kuh/col(2))
q2=3/2*a1*q1
q3=3*q1*a1*a2/(a1**3+2*a2**3)
put a1 into col(3)
put a2 into col(4)
put q1 into col(5)
put q2 into col(6)
put q3 into col(7)
cell(8,1)=1
cell(9,1)=cell(5,1)/2*dt/cell(8,1)
cell(10,1)=cell(6,1)/3*dt/cell(8,1)**2
cell(11,1)=cell(7,1)*dt

for i=2 to (n/dt)+1 step 1 do

if cell(2,i-1)>1350 then
cell(8,i)=cell(8,i-1)+cell(9,i-1)
cell(12,i)=1
end if
```

```
if cell(2,i-1)<=1350 and cell(8,i-1)<cell(3,i-1) and cell(8,i-1)<cell(4,i-1) then
cell(8,i)=cell(8,i-1)+cell(9,i-1)
cell(12,i)=1
end if

if cell(2,i-1)<=1350 and cell(8,i-1)>=cell(3,i-1) and cell(8,i-1)<cell(4,i-1) then
cell(8,i)=cell(8,i-1)+cell(10,i-1)
cell(12,i)=2
end if

if cell(2,i-1)<=1350 and cell(8,i-1)>=cell(4,i-1) then
cell(8,i)=cell(8,i-1)+cell(11,i-1)
cell(12,i)=3
end if

  cell(9,i)=cell(5,i)/2*dt/cell(8,i)
  cell(10,i)=cell(6,i)/3*dt/(cell(8,i)**2)
  cell(11,i)=cell(7,i)*dt
end for
```